CHAPTER II

THEORETICAL BACKGROUND AND LITERATURE REVIEWS

2.1 Elementary Processes in Photocatalysis Using Semiconductors

The principal characteristics involving in the activity of semiconductor photocatalysts are conduction band, valence band, band gap energy, trap site, and Fermi level. The bands are the allowed energy states that electrons can occupy in a photocatalyst molecule. The highest potential level occupied by electrons is called the valence band (VB), while the available lowest empty potential level next to the valence band is called the conduction band (CB). The bands are clearly differentiated in a semiconductor than that in a metal. The Fermi level is a probability distribution curve that represents 50% possibility of locating electrons at a given energy level. For n-type photocatalyst, such as TiO_2 and $SrTiO_3$, the Fermi level is close to the CB potential level, leading to the high probability of electron excitation by light irradiation. A pictorial representation of the band structure of a n-type photocatalyst is shown in Figure 2.1.
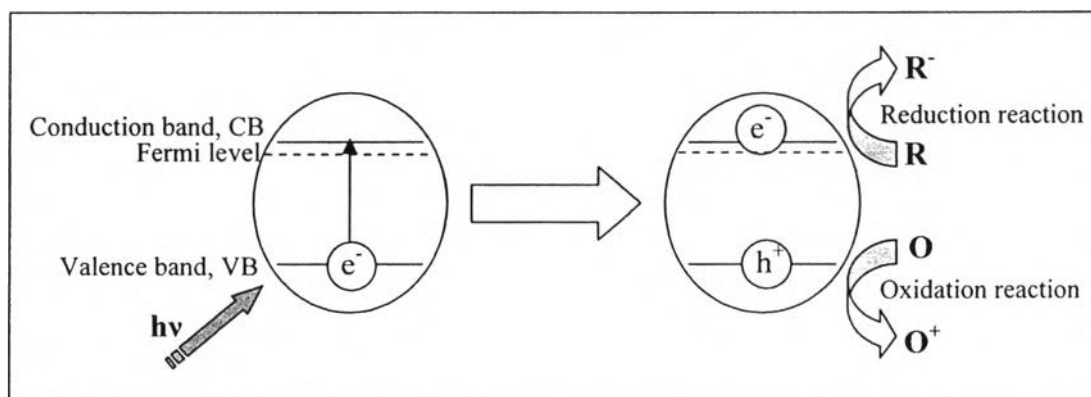

Figure 2.1 Electron-hole pair generation in a photo-irradiated n-type photocatalyst (Linsebigler *et al.*, 1995).

The band gap energy (E_g) is the energy difference between the CB potential level and the VB potential level (Linsebigler *et al.*, 1995). The band gap energy is usually calculated from the band gap wavelength (λ_g, nm):

$$E_g = \frac{hc}{\lambda_g} \tag{2.1}$$

where h is Planck's constant and c is the speed of light. The λ_g is the crossing point between the line extrapolated from the onset of the rising part and x-axis of the plot of the Kubelka-Munk function ($F(R)$) as a function of wavelength (λ, nm) (Kamat *et al.*, 1999), as shown in Figure 2.2.
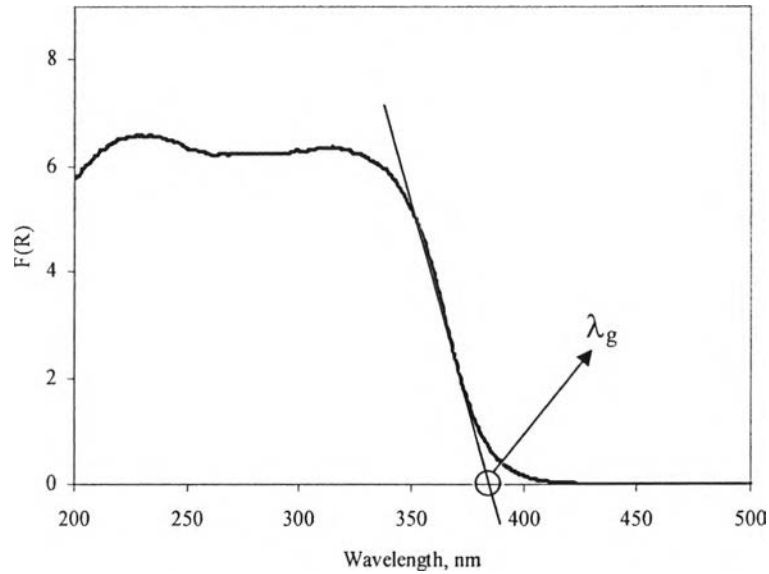

Figure 2.2 The plot between the Kubelka-Munk function ($F(R)$) as a function of wavelength (λ, nm) and the band gap wavelength (λ_g) estimation (Kamat *et al.*, 1999).
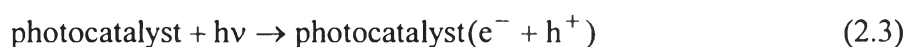
The Kubelka-Munk function ($F(R)$) can be expressed by the following equation:

$$F(R) = \frac{(1-R)^2}{2R} \tag{2.2}$$

where R is the ratio of the reflected light intensity of a sample to the reflected light intensity of the reference. All photons with $\lambda > \lambda_g$ cannot be absorbed and then

release as useless energy in the form of unproductive heat or photons. In addition, the band gap energy of any photocatalyst depends on its particle size. An increase in the band gap energy of a photocatalyst with a decrease in the particle size is defined as the quantization effect. Photocatalyst nanoparticles display this characteristic that alters their photochemical, photophysical, and photoelectrochemical properties. Both the large (e.g. ZnO, TiO_2, SnO_2, and WO_3) and the small (e.g. $CdSe$ and CdS) band gap photocatalysts can display this characteristic (Kamat, 1999; Anpo, 2004).

The mechanisms of photocatalyst-excitation initiated by light irradiation are as follows. Light with energy equal to and/or higher than the band gap energy of a photocatalyst can excite the electrons, resulting in the electron migration from the VB to the CB, leaving behind a hole in the VB, as shown in Figure 2.1 and Equation 2.3. The photo-generated electrons (e^-) and the photo-generated holes (h^+) are available for carrying out the redox activities at its surface. The photo-generated electron-hole pairs (e^--h^+ pairs) are also delocalized in the bulk of the photocatalyst. The delocalized locations are called trap sites. Unfortunately, the e^--h^+ pairs can undergo recombination, which results in decreasing the efficiency of the photocatalyst. The numbers of the useful e^- and h^+ in the photocatalyst are dictated by the ability of the surroundings to scavenge electrons and holes (Equation 2.4a and 2.4b) and the recombination between the e^--h^+ pairs (Equation 2.5).

$$photocatalyst + h\nu \rightarrow photocatalyst(e^- + h^+) \qquad (2.3)$$

$$photocatalyst(e^- + h^+) + R \rightarrow photocatalyst(h^+) + R^- \qquad (2.4a)$$

$$photocatalyst(e^- + h^+) + O \rightarrow photocatalyst(e^-) + O^+ \qquad (2.4b)$$

$$photocatalyst(e^- + h^+) \rightarrow photocatalyst \qquad (2.5)$$

Two major drawbacks of the large band gaps of photocatalysts have been identified as the recombination of photo-generated charges (e^--h^+ pairs) and the limited light harvesting ability. These drawbacks result in the limitation in the economical usage of the photocatalyst. The recombination problem can be minimized by loading metal on a photocatalyst. The loaded metal behaves as a sink for the photo-generated electrons, leading to decreasing recombination. Sensitization with dyes is one of the most commonly used methods to overcome the limited light
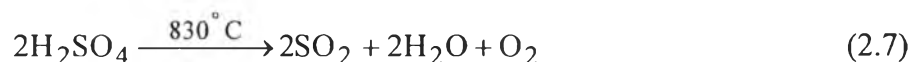
harvesting ability (Hotchandani and Kamat, 1992). Thus, both drawbacks of the photocatalyst can be effectively overcome by the modification of photocatalysts, depending upon the material used.

2.2 Hydrogen Production from Water

The life cycle of hydrogen is considerably clean and renewable because it can be produced from clean and renewable sources: water and sun light. Hydrogen is generated from water by a number of processes as follows:

2.2.1 Thermochemical Water Splitting With the Sulfur-Iodine Cycle (S-I Cycle)

The S-I cycle is a series of thermochemical processes used to produce hydrogen. The S-I cycle consists of three sequential chemical reactions, whose net reactant is water, and net products are hydrogen and oxygen.

$$I_2 + SO_2 + 2H_2O \xrightarrow{120^\circ C} 2HI + H_2SO_4 \qquad (2.6)$$

$$2H_2SO_4 \xrightarrow{830^\circ C} 2SO_2 + 2H_2O + O_2 \qquad (2.7)$$

$$2HI \xrightarrow{320^\circ C} I_2 + H_2 \qquad (2.8)$$

The sulfur and iodine compounds are recovered and reused, hence considering the process as a cycle. This S-I process is a chemical heat engine with an overall energy efficiency of around 50% (Kudo *et al.* 2004).

2.2.2 Direct Water Splitting at High Temperatures Using a Mixed Conducting Membrane

A mixed conducting membrane, such as ZrO_2-TiO_2-Y_2O_3 membrane, exhibits high ionic and electronic conductivity at high temperatures under low oxygen partial pressures. Using this system as a membrane for gas separation, hydrogen can be produced from direct water splitting at high temperatures. Vaporized water is dissociated at high temperatures, and the produced oxygen permeates through the membrane by the oxygen partial pressure difference. With

increasing oxygen partial pressure difference, the water splitting is promoted, and the amount of the produced hydrogen is increased. The concept of this process is shown in Figure 2.3. Water vapor is introduced into the right hand side of the membrane. At high temperatures greater than 1,300 K, water vapor begins to dissociate into species, such as H_2 and O_2. When the oxygen partial pressure on the left hand side of the membrane is lower than that of the right hand side, the dissociated oxygen permeates into the lower oxygen partial pressure side, leading to the separation between oxygen and hydrogen. Therefore, the recombination between hydrogen and oxygen does not take place. The use of the mixed conducting membrane has the advantage over the electrolysis because no electrodes or electric power are required (Cales and Baumard, 1984; Naito and Arashi, 1995).
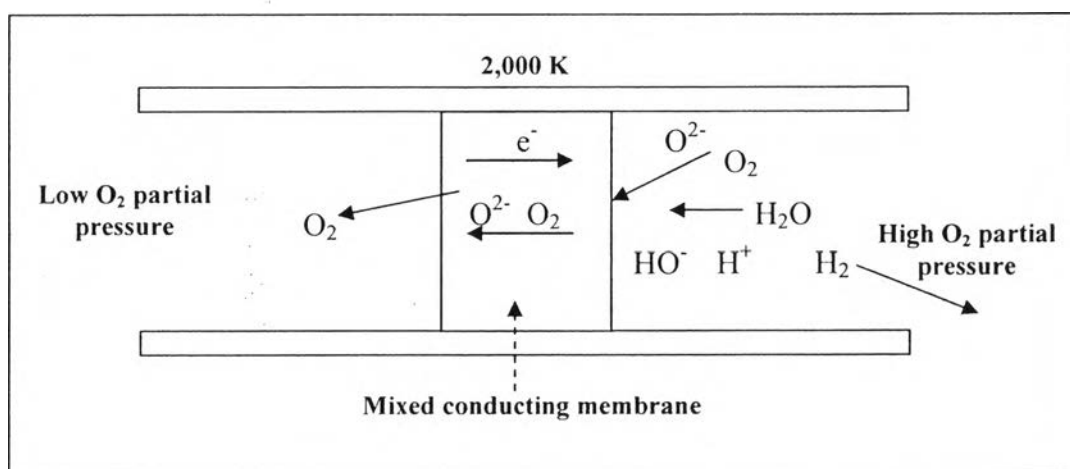

Figure 2.3 The concept of hydrogen production from direct water splitting at high temperatures using a mixed conducting membrane (Cales and Baumard, 1984).

2.2.3 Water Electrolysis

Electrolysis can be used to produce hydrogen by passing the direct current from a DC power supply into a bulk of water or electrolyte aqueous solution through electrodes. In electrolysis, the anode is the positive electrode, meaning that it has a deficit of electrons. The reactants in contact with the anode can then be oxidized. In the meantime, the cathode is the negative electrode, meaning that it has a surplus of electrons. The reactants in contact with the cathode tend to gain electrons

(can be reduced). For the platinum electrode, hydrogen gas is produced at the cathode, and oxygen is produced at the anode. If other metals are used as the anode, there is a chance that the oxygen will react with the anode instead of being released as a gas. For example, using iron electrodes in a sodium chloride solution electrolyte, iron oxide will be produced at the anode. The overall energy efficiency of water electrolysis varies widely around 25-40%. Figure 2.4 shows the Hoffman electrolysis apparatus used in the electrolysis of water.
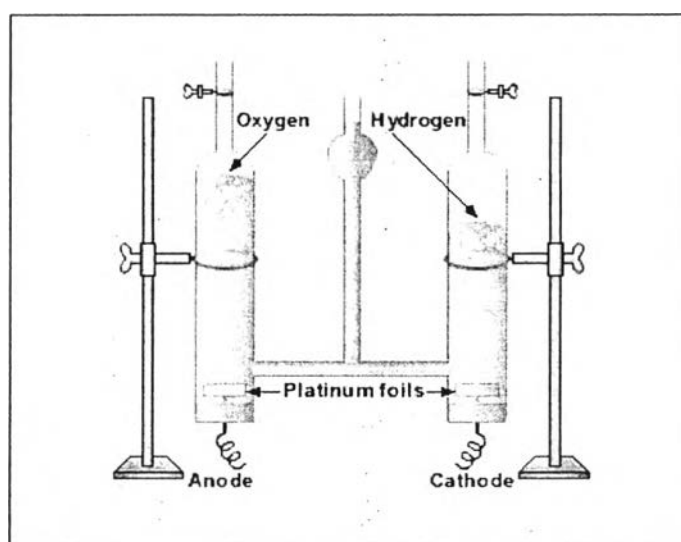

Figure 2.4 The Hoffman electrolysis apparatus used in electrolysis of water (www.hydrogen.co.uk)

2.2.4 High Temperature Electrolysis or Steam Electrolysis

The high temperature electrolysis is more efficient economically than traditional room-temperature electrolysis because some of the energy is supplied as heat, which is cheaper than electricity, and because the electrolysis reaction is more efficient at higher temperatures. The overall efficiency varies around 35-65%, depending upon the reaction temperature, where an increase in temperature leads to an increase in efficiency. The schematic of high temperature electrolysis is shown in Figure 2.5.
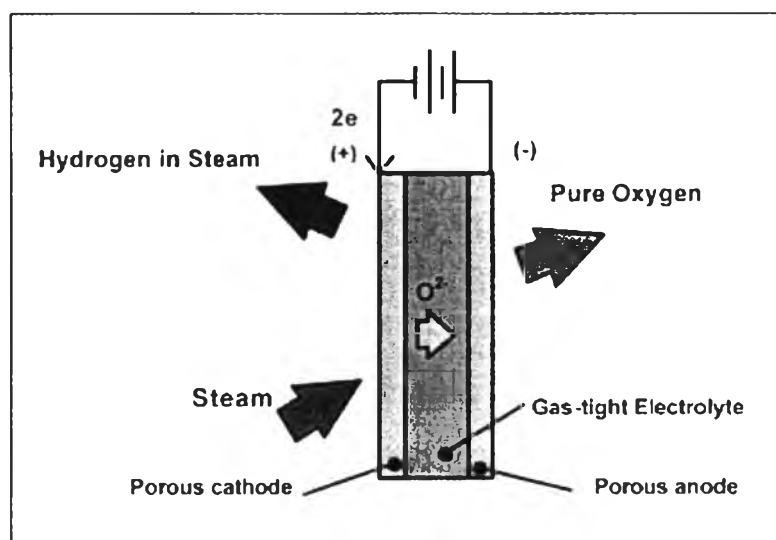
Figure 2.5 Schematic of high temperature electrolysis (www.hydrogen.co.uk).

2.2.5 Steam Reforming

The well-known commercial process, where methane (or natural gas) and steam are converted to syngas according to the following reaction, is called steam reforming.

$$CH_4 + H_2O(g) \xrightarrow{\quad 800-1000\,^{\circ}C \quad} 3H_2 + CO \qquad (2.9)$$

In the conventional process, natural gas is fed together with steam to the reformer, where the reforming reaction occurs over a catalyst at temperatures between 800 and 1000 °C.

2.2.6 Photocatalytic Decomposition of Water

The water decomposition reaction, as shown below;

$$H_2O \rightarrow H_2 + \tfrac{1}{2}O_2 \qquad (2.10)$$

is thermodynamically a two-electron process per molecule of hydrogen generated, with $\Delta G_0 = 237$ kJ mol^{-1} (Bolton, 1996; Ashokkumar, 1998). Thus, all hydrogen production processes from water always require the input energy, as shown in section 2.2.1 – 2.2.5. The processes that discussed above consume conventional sources of energy, such as petroleum, coal, and electricity. The burning of petroleum and coal

causes the emission of greenhouse gases and other pollutants as by-products, whereas for electricity source, the energy cost is very high with emission of greenhouse gases and other pollutants in some electricity production processes. Regarding these problems, the photocatalytic decomposition of water for hydrogen production is considered to a promising alternative. This is because photocatalysis is an environmentally friendly process that utilizes clean energy resource, i.e. solar energy, to perform the reactions. The photocatalytic reaction is originated by the direct absorption of a photon by the photocatalyst, and then the photo-generated electron-hole pairs are contributed to decompose water into H_2 and O_2 (Linsebigler et al., 1995). The electronic structure of the photocatalyst plays a key role in photocatalytic decomposition of water, depending upon the relative positions of the energy levels of the CB and VB with respect to protons reduction (H^+/H_2) and water oxidation (H_2O/O_2) potential levels and also depending upon the band gap energy (E_g). Theoretically, the energy difference of more than 1.23 eV is necessary in the photocatalytic decomposition of water because the thermodynamic potential, $E^{\circ}_{H_2O}$, for the water decomposition reaction (Zou et al., 2003; Licht et al., 2000) is given by:

$$E^{\circ}_{H_2O}(25^{\circ}C) = E^{\circ}_{O_2} - E^{\circ}_{H_2} = 1.23 \quad eV \qquad (2.11)$$

Photocatalysts, which have the energy levels of their CB potential level more negative than that of proton reduction level and their VB potential level more positive than that of water oxidation level, are possible to use to perform the photocatalytic decomposition of water to produce H_2 and/or O_2 in the presence of light irradiation (Honda and Fujishima, 1972), as shown in Figure 2.6. Some of the photocatalysts that satisfy both conditions are $SrTiO_3$, TiO_2, $Sr_2Nb_2O_5$, $Sr_2Ta_2O_7$, CdS, NiO, and etc. Their relative electronic structures with respect to H^+/H_2 and H_2O/O_2 potential levels are shown in Figure 2.7. One efficient photocatalyst for organic pollutants photodegradation and hydrogen production via photocatalytic water splitting is strontium titanium tri-oxide or strontium titanate ($SrTiO_3$).
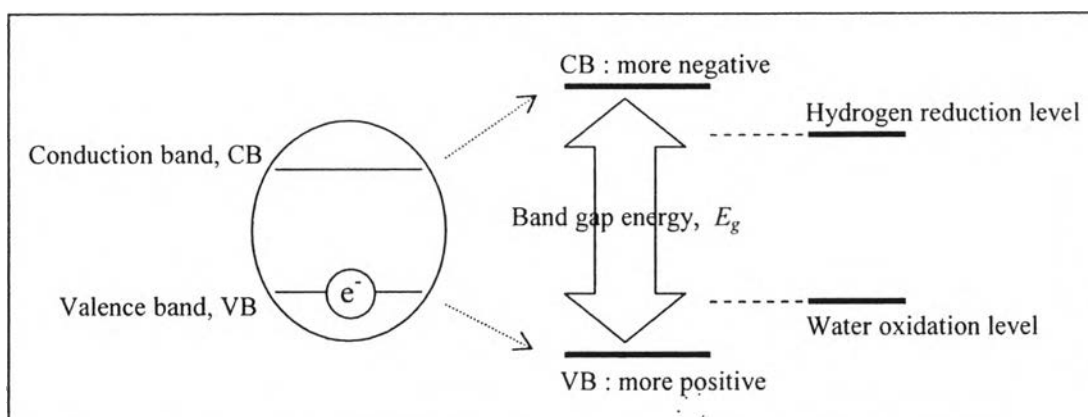
Figure 2.6 Band gap energy of the photocatalyst (Linsebigler *et al.*, 1995).
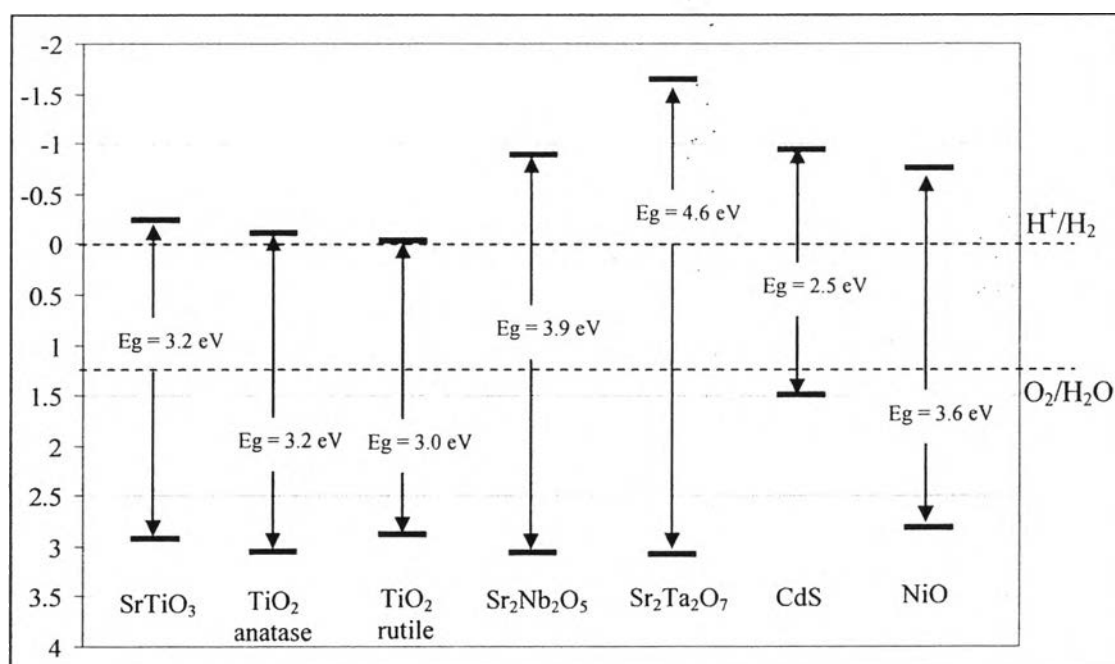
Figure 2.7 Band edge positions of semiconductors as determined in photoelectrochemical experiments with respect to a normal hydrogen electrode (NHE) as reference points, and the standard redox potentials of water in acidic condition (Meissner, 1999; Kudo *et al.*, 2000; Subramanian *et al.*, 2006).

As shown in Figure 2.7, $SrTiO_3$ is considered to be useful for photocatalytic decomposition of water in place of conventional photocatalysts, such as TiO_2 because its CB level provides a higher photopotential than TiO_2 and facilitates hydrogen and oxygen formation (Subramanian *et al.*, 2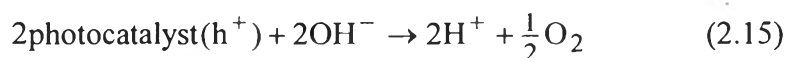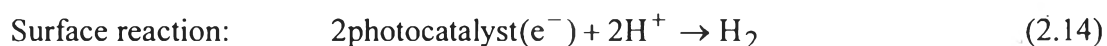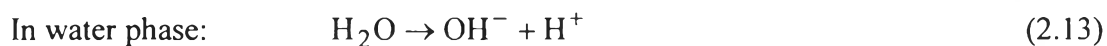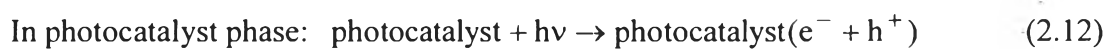006). Mover, $SrTiO_3$ photocatalyst exhibits the excellent properties such as its high photocorrosion resistibility, high thermal stability, strong hydrophilic surface, good host for metal doping, and high photocatalytic oxidative activity. Its metal-oxygen-metal angle of its crystal structure close to ideal bond angle for water splitting (the ideal bond angle is 180°.)(Blasse, 1998). Therefore, the focus of this research is on the use of $SrTiO_3$ photocatalysts for photohydrogen production from the photocatalytic decomposition of water and/or organic pollutants. The photocatalytic decomposition of water possibly takes place as the following chemical steps:

In photocatalyst phase: $\quad photocatalyst + h\nu \rightarrow photocatalyst(e^- + h^+)$ $\qquad$ (2.12)

In water phase: $\qquad H_2O \rightarrow OH^- + H^+$ $\qquad$ (2.13)

Surface reaction: $\qquad 2photocatalyst(e^-) + 2H^+ \rightarrow H_2$ $\qquad$ (2.14)

$\qquad\qquad\qquad\qquad 2photocatalyst(h^+) + 2OH^- \rightarrow 2H^+ + \frac{1}{2}O_2$ $\qquad$ (2.15)

The overall reaction: $\quad H_2O + 2h\nu \xrightarrow{\quad photocatalyst \quad} H_2 + \frac{1}{2}O_2$ $\qquad$ (2.16)
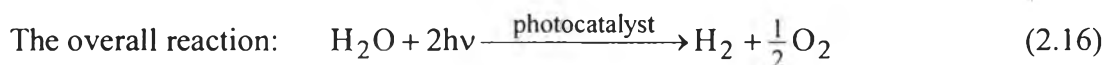
The reduction and oxidation reactions are the basic mechanisms of photocatalytic hydrogen production. Without light irradiation or no excitation, both the electrons and holes are in the VB. When photocatalysts are excited by photons with the energy equal to or higher than their band gap energy, electrons in the VB which receive sufficient energy from the photons are promoted to the CB. These photo-generated electrons become important as their role to reduce the protons to hydrogen molecules (Equation 2.14), and the photon-generated holes simultaneously generate O_2 (Equation 2.15) or free radicals, which are able to undergo the secondary reaction. The photo-generated electrons and holes that migrate to the surface of the photocatalyst without recombination reduce protons and oxidize water that both are adsorbed on the photocatalyst surface. The electrons and holes can also recombine in the bulk phase or on the surface of the photocatalyst within a very short time,

resulting in low energy conversion efficiency from the solar energy to hydrogen by the photocatalytic decomposition of water. The low energy conversion efficiency of photocatalytic decomposition of water for hydrogen production is mainly due to the following reasons:

- Recombination of photo-generated electron-hole pairs: CB electrons can recombine with VB holes very quickly, and the recombination releases useless energy in the form of unproductive heat or photons.

- Fast backward reaction: the decomposition of water into hydrogen and oxygen is an energy-consuming process, thus the backward reaction (the recombination of hydrogen and oxygen into water) easily proceeds.

- Limited light harvesting ability: most photocatalysts have a bang gap energy wider than 3 eV that does not suit with visible light radiation ($\lambda \geq 420$ nm), which is the large fraction of solar radiation.

In order to solve the above problems, attempts have focused on promoting the photocatalytic activity and enhancing the visible light response. An addition of hole scavengers (electron donors), noble metal loading, metal ion doping, anion doping, dye sensitization, composite semiconductor photocatalyst, etc., have been investigated, and some of them have been proved to be useful to enhance hydrogen production. The above listed techniques influencing H_2 production have been grouped under two broad classifications as chemical addition and photocatalyst modification.

2.3 Chemical Addition for H_2 Production Enhancement

2.3.1 Hole Scavenger Reagents to Suppress Electron-Hole Recombination

Due to the rapid recombination of photo-generated electrons and holes, it is difficult to achieve photocatalytic decomposition of water for hydrogen production using active photocatalysts, such as TiO_2 and $SrTiO_3$, from distilled water. Adding some specific chemical additives into distilled water can enhance the photo-generated electron-hole separation, resulting in higher photocatalytic activity. This enhancement is obtained because the chemical additive behaves as a hole scavenger, which can react irreversibly with the photo-generated holes. Hence, the chemical

additives for the photocatalytic decomposition of water can be considered as a hole scavenger reagent. Due to the ability to enhance the photocatalytic activity of a hole scavenger, many researchers have continued to investigate the use of hole scavengers. Sayama *et al.* (2000) studied the effect of sodium salt addition on the rate of photocatalytic decomposition of water into H_2 and O_2 using a Pt-loaded TiO_2 photocatalyst. In the case of no addition, a small amount of H_2 was evolved, but O_2 evolution was not observed. Upon the addition of a sodium salt, such as NaOH, NaCl, $NaHPO_4$, Na_2SO_4, Na_2CO_3, and Na_3PO_4, the H_2 evolution rate increased in comparisons with the case of no addition, but the H_2 evolution rate was not highly maintained at long irradiation time due to the adsorption of salts on photocatalyst surface. Among all types of studied sodium salts, the addition of Na_2CO_3 resulted in dramatically an increasing H_2 evolution rate. The photocatalytic production of hydrogen on $Pt/SrTiO_3$ suspended in ethylene diamine tetraacetic acid (EDTA), triethanolamine (TEOA), or $H_2PO_2^-$ solution was investigated by Avudaithai and Kutty (1987). $H_2PO_2^-$ was more effective than EDTA and TEOA. This was in contrast to the use of TiO_2 as the photocatalyst, where EDTA was better than other hole scavengers (Kutty and Avudaithai, 1988). Other organic compounds were also used as hole scavenger reagents. Li *et al.* (2003) investigated the photocatalytic H_2 production from Pt/TiO_2 suspension in the presence of $H_2C_2O_4$, HCOOH, and HCHO, and found that the H_2 production efficiency with these hole scavengers decreased in the following order: $H_2C_2O_4$ > HCOOH > HCHO. Takata *et al.* (1998) reported the photocatalytic decomposition of water over various photocatalysts, such as TiO_2, $SrTiO_3$, Ta_2O_5, and etc., in both aqueous Na_2CO_3 solution and distilled water. Na_2CO_3 was found to efficiently enhance the photocatalytic decomposition of water. They also reported the effect of alcohol (as hole scavenger) on the photocatalytic H_2 production over Pt/TiO_2. The H_2 production efficiency decreased in the following order: ethanol > methanol > 1-propanol > 1-butanol. In addition, their results showed that the difference in the photocatalysts caused the difference in the sequence of efficiency induced by these alcohols. For example, for $Pt/KCa_2Nb_3O_{10}$ photocatalyst, the H_2 production efficiency decreased in the following order: methanol > ethanol > 1-propanol > 1-butanol.

2.3.2 Chemical Additives to Suppress the Backward Reaction of H_2 and O_2

As previously mentioned, another main problem is the fast backward reaction of H_2 and O_2 due to an energy-consuming process of the decomposition of water into H_2 and O_2. Some researchers investigated the chemical additives that are capable of reducing this problem. Sayama and Arakawa (1992, 1994, 1996, 2000) reported that an addition of carbonate salts could significantly enhance H_2 and O_2 production. Various semiconductor photocatalysts, including TiO_2, $Pt-TiO_2$, Ta_2O_5, and ZrO_2, were tested, and it was found that the presence of Na_2CO_3 was very beneficial for H_2 and O_2 production for all the photocatalysts tested. The results from the Infrared (IR) study in the case of Pt-loaded TiO_2 revealed that the surface of Pt-loaded TiO_2 was covered by many types of carbonate species. Therefore, photo-generated holes were consumed by reacting with carbonate species to form carbonate radicals, which is beneficial for photo-excited electron-hole separation. On the other hand, peroxycarbonates were easily decomposed into O_2 and CO_2. The evolution of CO_2 and O_2 could promote desorption of O_2 from the photocatalyst surface and thus could minimize the formation of H_2O through the backward reaction of H_2 and O_2.

An addition of iodide was also found to be advantageous for hydrogen production. Iodide anion (I^-) in a suspension could adsorb preferentially onto Pt surface, forming an iodine layer. The iodine layer can thus suppress the backward reaction of H_2 and O_2 to form H_2O (Abe et al., 2003). Sayama et al. (2002) found that the H_2 evolution took place on Pt-loaded Cr-Ta-doped $SrTiO_3$ using I^- (NaI aqueous solution) under visible light irradiation. However, adding too much carbonate salt or iodide anion beyond an optimum level was found to reduce the beneficial effects, since these species adsorbed onto the photocatalyst surface can decrease light harvesting ability (Sayama and Arakawa, 1996).

2.4 Photocatalyst Modification for H_2 Production Enhancement

2.4.1 Ion Doping

2.4.1.1 Metal Ion Doping

Metal ion doping is an interesting method for developing visible light-driven photocatalysts. The metal ions doped are incorporated into the

lattice of a photocatalyst, leading to a change in the electronic structure of the photocatalyst and resulting in improving the visible-light absorption ability. The drawback of this modified method is that the doping metal ions also work as a recombination center between the photo-generated electrons and the photo-generated holes, somewhat resulting in the decrease in the photocatalytic activity. Perovskite $SrTiO_3$ has been recently reported to be one of the host materials for the design and development of visible light-driven photocatalysts, whereas $SrTiO_3$ alone is active only under UV radiation. The substitution of the Sr^{2+} or Ti^{4+} with a metal cation is expected to alter the electronic structure. The doping of a metal cation can alter the band structure of $SrTiO_3$, if the size of the doping metal ion is compatible with the lattice size of the perovskite. Several metals such as Ag, Cr, Pt, Rh, Pd, and Ta are incorporated well into $SrTiO_3$. The photocatalytic activity enhancement by Ag doping on $SrTiO_3$ was reported by Subramanian *et al.* (2006). $SrTiO_3$ doped with Cr^{3+} led to an introduction of isolated energy levels within its band gap, so photons can be absorbed at the two levels, the band gap and the sub-band gap, where the latter leads to the light absorption improvement in the visible region (Ashokkumar, 1998). In addition, Ru-, Rh-, Ir-doped $SrTiO_3$ photocatalysts were found to possess an intense absorption band in the visible light. The visible light response is due to the transition from the electron donor level formed by the dopant ions to the conduction band composed of Ti3d orbitals of $SrTiO_3$. The Ru-, Rh-, Ir-doped $SrTiO_3$ loaded with Pt co-catalyst exhibited the photocatalytic activity for H_2 production from an aqueous methanol solution under visible light irradiation (Konta *et al.*, 2004; Kudo, 2006). Ishii *et al.* (2004) also studied the $SrTiO_3$ photocatalysts doped with chromium ion. Their photocatalysts showed the photocatalytic activity for H_2 evolution from an aqueous methanol solution under visible light irradiation with a long induction period. The long induction period could cause by an increase in the e^--h^+ recombination through the reduction process of forming Cr^{3+} and/or Cr^{4+} from Cr^{6+} and the oxygen defects. The Cr^{6+} ions and oxygen defects were formed to maintain charge balance when Ti^{4+} ions in $SrTiO_3$ lattice were replaced by Cr^{3+} ions. They concluded that the charge balance by the change compensation between the doped metal ions was a significant effect on the photocatalytic activity as shown by the increase in the activity and the decrease in the induction period of the Cr^{3+}/Ta^{5+}-

doped $SrTiO_3$ when compared with the Cr^{3+}-doped $SrTiO_3$. It is because the Cr^{6+} ions and oxygen defects are suppressed by co-doping of tantalum ions since the charge balance in lattice is maintained by the substitution of a couple of Cr^{3+}/Ta^{5+} for two Ti^{4+} ions.

2.4.1.2 Anion doping

The use of anion doping to improve hydrogen production under visible light is a new approach. Doping of anions (N, F, C, S, etc.) in the crystalline structures of some photocatalysts can shift the photo-response into visible region. Unlike metal ions (cations), anions less likely form recombination centers and, therefore, are more effective to enhance the photocatalytic activity (Asahi et al., 2001; Umebayashi et al., 2002; Ohno et al., 2004; Torres et al., 2004). Asahi et al. (2001) studied the substitutional doping contents of C, N, F, P, and S for the O atoms in anatase TiO_2. It was found that mixing of p state of N with 2p of O could shift the VB edge upwards to narrow down the band gap of TiO_2. The doping of S was found to result in a similar band gap narrowing. This is because the ionic radius of S is too large to be incorporated into the lattice of TiO_2. The doping of C or P was found to be less effective because the doped location is so deep that the photo-generated charge carriers are difficult to migrate to the surface of the photocatalyst. Tsuji et al. (2003) investigated the effect of co-doping of halogen (Cl, Br, and I) anions into a Pb-ZnS photocatalyst. The doping of halogen ions may be useful for the relaxation of the distortion by the doping of large Pb cations and suppress the formation of non-radiative transition site, at which the recombination between photo-generated e^- and h^+ likely occurs. The photocatalytic activity of Ni- or Cu-doped ZnS was increased about 20% by the co-doping of a halogen anion. On the other hand, the activity of the halogen-co-doped photocatalyst was drastically increased about three times higher than that of the non-halogen-co-doped photocatalyst. Wang et al. (2004) investigated the effect of nitrogen doped into a $SrTiO_3$ photocatalyst via on the photocatalytic elimination of NO gas. The results showed that the photocatalytic activity of the $SrTiO_3$ could be greatly improved by nitrogen doping. Its photocatalytic activity under light irradiation with $\lambda > 400$ nm was about 3.5 and 1.4 times higher than those of native $SrTiO_3$ and commercial titania powder (Degussa P-25).

2.4.2 Metal or Co-Catalyst Loading

Regarding the photocatalytic reactions, the charge (e^--h^+) transfer is as important as the charge separation. Because the photocatalytic reaction can occur only when the photo-generated e^- and h^+ migrate to the surface sites, ions should be doped near the surface of photocatalyst particles for a better charge transfer. If the ions are deeply doped, they likely behave as recombination centers, since the e^--h^+ migration to the photocatalyst surface is more difficult. Another method that is used to enhance the photocatalytic activity by increasing the charge transfer is metal or co-catalyst loading. The loaded metal or co-catalyst acts as a charge transferring site and/or active site for the photocatalytic reactions. It was reported that the photocatalytic activity of TiO_2 could be remarkably enhanced by the addition of a small amount of Pt. Such an enhancement in the photocatalytic activity has been explained by the photoelectrochemical mechanism, in which the photo-generated electrons quickly transfer to the Pt particles loaded onto the TiO_2 surface where the proton reduction reaction proceeds. In this case, Pt behaves as both charge transferring site and active site (Anpo, 2004). This behavior of Pt-loaded on TiO_2 photocatalyst was confirmed by such as the study of the photocatalytic degradation of 2-propanol (Chavadej et al., 2008). Their results showed that the photocatalytic activity of Pt-loaded TiO_2 was much higher than that of either Pt metal or TiO_2 photocatalyst. They pointed out that the increase in the photocatalytic activity was caused by the Pt nanoparticles on TiO_2 surface, which were responsible for providing the adsorption sites of 2-propanol and reducing the electron/hole recombination. Sayama et al. (2002) found that the H_2 evolution took place on Cr-Ta-doped $SrTiO_3$ photocatalysts with using I^- as a hole scavenger (NaI aqueous solution) under visible light and the photocatalytic activity was drastically increased with loading Pt onto the Cr-Ta-doped $SrTiO_3$ photocatalyst. Domen et al. (1986) reported the photocatalytic H_2 production over NiO-loaded $SrTiO_3$ photocatalysts. The photocatalytic activity was enhanced (when compared with native $SrTiO_3$) via two possible mechanisms: first mechanism, the electrons in the CB of $SrTiO_3$ were transferred directly to the Ni metal particles and then transferred to H^+, which adsorbed on the NiO site. For the second mechanism, both NiO and $SrTiO_3$ are excited by photon, and the hole in the VB of $SrTiO_3$ involves in the water oxidation,

while the electrons in the CB of NiO involve in the H^+ reduction, and the hole in the VB of NiO and the electrons in the CB of $SrTiO_3$ are combined at the Ni site. Qin *et al.* (2007) studied the influence of CoO co-catalyst on the photocatalytic activity of La-doped $SrTiO_3$ and pointed out that the increase in the photocatalytic activity was due to the role of Co metal, which should remain at an inner core of the $SrTiO_3$, might be to capture the electrons from the n-type semiconductor $SrTiO_3$ and the holes from the p-type CoO, and to prevent the recombination. The influence of loading amount of CoO co-catalyst on the photocatalytic activity was also studied and their results showed that the optimum loading amount of CoO increased with increasing the faction of La doping. The other perovskite type photocatalysts, such as $Sr_2Ta_2O_7$, showed the activities of water splitting into H_2 and O_2 in pure water without any additives under UV irradiation. The activity of $Sr_2Ta_2O_7$ was much increased by loading NiO as a co-catalyst even without pretreatment. On the other hand, native $Sr_2Nb_2O_7$ did not possess the activity. The high activity was obtained for the $Sr_2Nb_2O_7$ photocatalyst when NiO was loaded and pretreated. A predominant factor affecting the photocatalytic behavior of $Sr_2Ta_2O_7$ and $Sr_2Nb_2O_7$ is the conduction band levels formed by Ta5d and Nb4d (Kudo *et al.*, 2000). In addition, Sreethawong *et al.* (2005a, b) also investigated the effect of NiO co-catalyst loaded on mesoporous TiO_2 and Ta_2O_5 photocatalysts for the photocatalytic decomposition of water in an aqueous methanol solution. They also found that the photocatalytic performance of both mesoporous photocatalysts was improved by the presence of the loaded NiO co-catalyst.

2.4.3 Dye Sensitization

The charge transfer from light-excited organic molecules (dyes) to a semiconductor with a large band gap has long been known. This technique involves in both photoelectrochemistry and photocatalysis areas, in the recent year, and known as dye sensitization. Under visible light irradiation, the excited dyes can inject electrons to the CB of a semiconductor photocatalyst to initiate the catalytic reactions, as shown in Figure 2.8. According to the mechanism of dye sensitization, the fast electron injection and slow electron/hole recombination are the properties that are required to achieve a higher efficiency in energy conversion. Based on the literature

on electron/hole recombination of dyes, the recombination times were found to be mostly in the order of nanoseconds to microseconds, sometimes in milliseconds (Hannappel *et al.*, 1997; Martini *et al.*, 1998; Yan and Hupp, 1996), while the electron injection times were in the order of femtoseconds (Burfeindt *et al.*, 1996; Rehm *et al.*, 1996; Martini *et al.*, 1998). The fast electron injection and slow electron/hole recombination make dye sensitization sufficient for enhancing the overall energy conversion of the photocatalytic reaction due to enhancing the visible light absorption of large band gap photocatalysts.
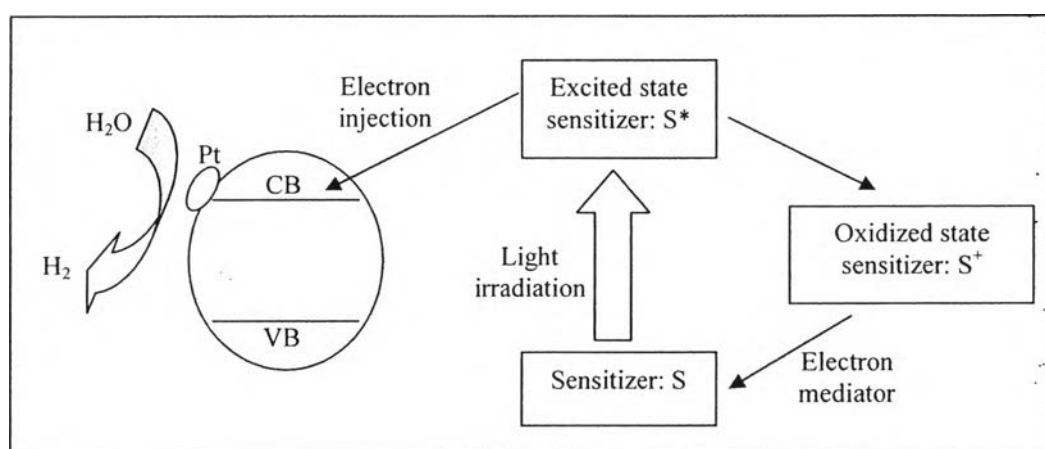

Figure 2.8 Mechanism of dye-sensitized photocatalysis under light irradiation (Ashokkumar, 1998).

For example, the adsorption of dye sensitizers, such as $Ru(bpy)_3^{2+}$, Eosin Y, Merocyanine, and Coumarin dyes, etc., on platinized TiO_2 photocatalyst led to efficient H_2 evolution from water under visible light in the presence of sacrificial reagents, such as TEAO, EDTA, acetonitrile, and aqueous I^- solution (Kiwi and Gratzel *et al.*, 1979; Kajiwara *et al.*, 1982; Wang *et al.*, 2003; Abe *et al.*, 2004). Even without semiconductor photocatalysts, some dyes, such as Safranine-O/EDTA, and Safranine-T/EDTA, are able to absorb visible light and produce electrons as reducing agents strong enough to produce hydrogen (Bi and Tien, 1984). Nevertheless, without photocatalysts, the rate of hydrogen production merely by dyes is very low. Gurunathan *et al.* (1997) investigated the effects of different dyes on the

photocatalytic hydrogen production by SnO_2. Qualitatively, the ranking of dyes in terms of the degree of enhancement of hydrogen production rate was found in the following order: Eosin Blue > Rose Bengal > $Ru(bpy)_3^{2+}$ > Rhodamine > Zacriflavin > Fluorescein. Memming *et al.* (1983) pointed out that only the first monolayer of dyes directly adsorbed on the semiconductor photocatalyst surface is able to inject charge carriers into the photocatalysts.

2.4.4 Composite Semiconductor Photocatalysts

The use of semiconductor photocatalyst composites (coupling) is one method to utilize visible light for hydrogen production. When a large band-gap semiconductor is coupled with a small band gap semiconductor with a more negative CB level, the CB electrons can be injected from the small band gap semiconductor to the large band gap semiconductor. The wide electron-hole separation is achieved and thus generates more charges to perform photocatalysis (Kudo, 2006). The process is quite similar to dye sensitization. The difference is that electrons are injected from one semiconductor to another semiconductor, rather than from excited dye to semiconductor, as shown in Figure 2.9.
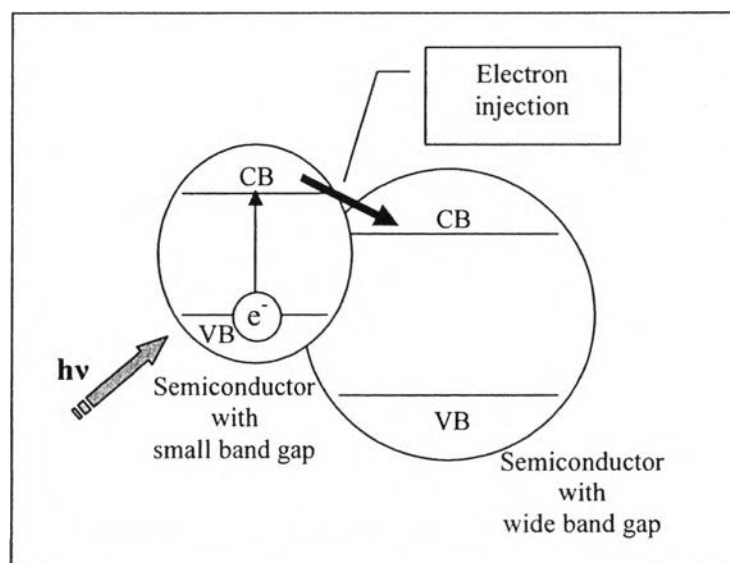

Figure 2.9 Electron injection in composite semiconductors (Ashokkumar, 1998).

Successful coupling of two semiconductors for the photocatalytic water splitting for hydrogen production under visible light irradiation can be achieved when the following conditions are met:

- The small band gap semiconductor should be able to be excited by visible light,

- The CB of the small band gap semiconductor should be more negative than that of the large band gap semiconductor,

- The CB of the large band gap semiconductor should be more negative than proton reduction level and

- The electron injection should be fast as well as efficient.

Jang *et al.* (2007) reported that CdS(bulk)/TiO$_2$ composite photocatalysts showed a high photocatalytic activity for hydrogen production from an electrolyte solution containing sulfide and sulfite as sacrificial reagents under visible right irradiation ($\lambda \geq 420$ nm). Its activity was much higher than that of single CdS photocatalyst. The superior activity of the composite photocatalyst is considered to be due to a fast charge separation. Thus, the difference in the positions of conduction bands drives photoelectrons generated in bulky CdS upon initial light absorption to surrounding TiO$_2$ nanoparticles. The optimum molar concentration of TiO$_2$ in CdS(bulk)/TiO$_2$ that showed the highest activity for H$_2$ evolution was determined to be 0.67. So *et al.* (2004) also conducted photocatalytic hydrogen production using CdS/TiO$_2$ composite semiconductors and concluded that the photocorrosion of CdS can be prevented by addition of Na$_2$S. De *et al.* (1996) conducted solar photocatalytic hydrogen production using CdS/ZnS composite semiconductors. They showed that the addition of n-Si into CdS/ZnS photocatalyst enhanced hydrogen production rate. This is due to the smaller band gap of n-Si together with its more negative CB. When exposed to solar radiation with wavelength longer than 520 nm, electrons are excited from the VB of n-Si to the CB of n-Si and then transferred to the CB of CdS sequentially, resulting in a higher solar radiation utilization. They also showed that the photocorrosion of CdS could be inhibited by addition of Na$_2$S/Na$_2$SO$_3$ into the solution.

In addition, Jin *et al.* (2007) applied the dye sensitization with the photocatalyst composite technique to prepare an Eosin Y-sensitized CuO/TiO$_2$

photocatalyst. The photocatalytic activity of the CuO/TiO_2 photocatalyst for hydrogen production was significantly enhanced by Eosin Y sensitization due to the build-up of excess electrons in the conduction band of CuO by the excited electrons from both sensitizer molecules and TiO_2 that were injected into the CB of CuO through the CB of TiO_2.

2.4.5 Structure and Morphology Control of Photocatalysts

The structure and morphology are the important characteristics of photocatalysts that affect their photocatalytic activity, as described in many researches. The photocatalytic activity enhancement by the presence of mesoporosity was reported. Basca and Kiwi (1998) reported that the presence of the rutile phase in TiO_2 causing mesoporosity and wide pore size distribution, which gave rise to higher photocatalytic activity. Dai et al. (1999) showed that the mesostructured TiO_2 had much higher photocatalytic activity for the degradation of 2,4,6-trichlorophenol (TCP) in water than non-mesostructured TiO_2 nanoparticles (P-25). Moreover, the enhancement of the photocatalytic activity of different photocatalysts was also confirmed by the presence of mesoporosity (Sreethawong et al., 2005a, b, c, 2006). Wang et al. (2007) prepared fibrous $SrTiO_3$ photocatalysts by using the hydrothermal reaction method. Their fibrous $SrTiO_3$ exhibited higher NO elimination capability than the spherical $SrTiO_3$ prepared by the solid-state reaction. For their N-doped fibrous $SrTiO_3$, it showed excellent photocatalytic activity, which was about 2.4 times higher than that of spherical $SrTiO_3$ powders for the irradiation with $\lambda > 400$ nm and about 1.3 times higher than that of a spherical one for the irradiation with $\lambda > 290$ nm. Ikeda et al. (2006) investigated a novel phase-boundary photocatalyst for overall water splitting. They prepared a Pt-loaded $SrTiO_3$ (core)-silica (shell) photocatalyst and modified it with a fluoroalkylsilylation agent to obtain the floated powder photocatalyst. The obtained photocatalyst could assemble at a gas–water interface in the water splitting system. The overall efficiency of this system was higher than that of the non-floated Pt-loaded $SrTiO_3$ suspension system. The higher efficiency is probably due to the suppression of the backward reaction (the production of water from H_2 and O_2) by the fast diffusion rate of produced gases

from water phase into gas phase that was induced by the floated photocatalyst. However, this novel phase-boundary photocatalyst showed low photostability.

When considering the crystal structure, the ideal Metal-Oxygen-Metal (M-O-M) bond angle of 180° of photocatalyst is very benefit for photoexcitation due to the ideal lowest excitation energy and the easy electron localization (Blasse, 1998). Thus, many researchers turn to investigate the perovskite-type photocatalysts because the M-O-M bond angle in crystal structure are close to the ideal bond angle (180°), especially $SrTiO_3$ which has an ideal cubic perovskite crystal structure, as shown in Figure 2.10. The Ti-O-Ti bond angle in the cubic perovskite $SrTiO_3$ is very close to the ideal bond angle.
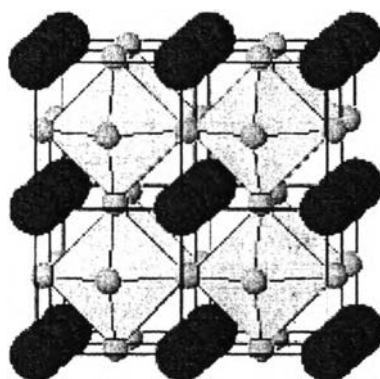

Figure 2.10 Cubic perovskite $SrTiO_3$ (Blasse, 1998).

The perovskite structure can be represented by the general formula; ABO_3, in which A, the large cation site, may be an alkali, alkaline earth, or rare-earth ion, and B, the small cation site, is a transition metal cation. The ideal perovskite structure is cubic. A large number of the ABO_3 compounds are orthorhombic, rhombohedral, or tetragonal but are so close to cubic that they can be approximated by the cubic structure. The perovskite structure provides the flexibility to vary the composition of the A and B sites and/or to incorporate a combination of cations at the A and B sites to form substituted perovskites. Because the crystal structure of perovskite compounds is primarily determined by ionic size rather than valency, it is possible to substitute selectively for either the A or B ion by introducing isovalent or

aliovalent ions. If the ionic radius of a substitute cation is close to the native cation in an oxide, the substitution can occur even though the valence of the ions may be different. If the valence is different, compensating electrons, holes, or charged vacancies will occur, leading to the change in their electrochemical properties. Thus in principle, for the perovskite-structured photocatalysts, the adjustment of the stoichiometry and/or doping with isovalent or aliovalent ions can be used to modify their photocatalytic properties (Kudo et al., 2000; Suzuki et al., 2005; Subramanian et al., 2006; Qin et al., 2007). For example, Subramanian et al. (2006) investigated the stoichiometry (Sr-to-Ti) effect on the photocatalytic activity of SrTiO$_3$ in the photodegradation of victoria blue dye. The SrTiO$_3$ photocatalyst with an equimolar Sr-to-Ti ratio exhibited higher photocatalytic activity than the non-equimolar Sr-to-Ti ratio SrTiO$_3$ photocatalyst. In addition, for the native perovskite-structured photocatalysts, it was reported that the dipole moment along perovskite layers seemed to enhance the charge separation, resulting in high photocatalytic activity (Kudo et al., 2000). Table 2.1 summarizes the results of hydrogen production efficiency using SrTiO$_3$ at different loading metals and operational conditions. From Table 2.1, the SrTiO$_3$ with La and CoO doped give the highest hydrogen production.

2.5 Photocatalytic Degradation of Organic Pollutants

Photocatalysts can also be applied for the photodegradation of various organic pollutants, as mentioned in Section 2.2. Ahuja and Kutty (1996) investigated the photocatalytic activity of SrTiO$_3$ for the photodegradation of phenol in an aqueous solution. The SrTiO$_3$ photocatalyst showed higher photocatalytic activity than the commercial TiO$_2$ (Degussa P25). Otsuka-Yao-Matsuo et al. (2004) investigated the photobleaching of methylene blue aqueous solution by using TiO$_2$, SrTiO$_3$, CeTiO$_4$, CeTi$_2$O$_6$, TiO$_2$/SrTiO$_3$, CeTiO$_4$/SrTiO$_3$, and CeTi$_2$O$_6$/SrTiO$_3$ photocatalysts, and their results showed that the photocatalytic activity of those photocatalysts were relatively high under visible light irradiation. Wang et al. (2004, 2007) prepared fibrous SrTiO$_3$ photocatalyst by using the hydrothermal reaction method. Their fibrous SrTiO$_3$ exhibited higher NO elimination capability than the spherical SrTiO$_3$ prepared by the solid-state reaction. For the N-doped fibrous

$SrTiO_3$, it showed excellent photocatalytic activity, which was about 2.4 times higher than that of spherical $SrTiO_3$ powders for $\lambda > 400$ nm and about 1.3 times higher than that of a spherical one for $\lambda > 290$ nm.

There is another option for combining photodegradation of organic pollutants and the hydrogen production, as indicated in the following equation.

$$CH_3COOH(aq) + O_2 \rightarrow 2CO_2(g) + 2H_2(g)$$
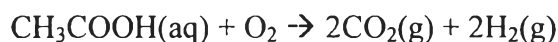
Acetic acid (CH_3COOH) is used as the sacrificial donor in the reduction half reaction. Hydrogen is directly produced at the same time as this organic compound is oxidized (Bolton, 1996). The photoinduced hydrogen production from the photocatalytic degradation of a number of organic compounds in solution, including alcohols and organic acids, has been investigated under solar or UV irradiation with the use of Pt/TiO_2 photocatalyst (Patsoura, 2007). It has been found that the rate of photoinduced hydrogen production depends strongly on the concentration of the sacrificial agent employed and to a lesser extent on solution pH and temperature. At this point, it can be concluded that photodegradation of organic pollutants (such as alcohols and organic acids) can be achieved with simultaneous production of H_2, and this process potentially provides an efficient and cost effective method for the waste treatment.

In addition, in the case that the final decomposed products are CO_2 and H_2O (Barreto et al., 1996; Pozdnyakov et al., 2004; Hoffmann et al., 2008), the potentially added value of hydrogen production is possible. It is therefore possible to modify these photodegradation processes with photocatalytic hydrogen production, whereas hydrogen would be produced from the organic pollutants during the photodegradation processes. Table 2.2 summarizes the results of photodegradation of various pollutants using $SrTiO_3$ with various modifications.

Table 2.1 Results of the SrTiO$_3$-based photocatalysts for photocatalytic decomposition of water for hydrogen production

No.	Photocatalyst	Reaction Conditions (amount of catalyst, reactant solution, light source)	Irradiation type	Hydrogen evolution, $\mu mol \cdot h^{-1}$	References
1	1% Rh-doped, 0.1 wt.% Pt-loaded SrTiO$_3$	Photocatalyst: 0.3 g. 150 ml of 10 vol.% aqueous MeOH, 300 W Xe lamp with cutoff filter (λ > 440 nm)	Top irradiation	117 (maximum rate)	Konta *et al.*, 2004
2	4 mol% Cr-, 4 mol% Ta-1 wt.% Pt-loaded SrTiO$_3$, with H$_2$ reduction at 773 K	Photocatalyst: 1 g. 310 ml of 6.5 vol.% aqueous MeOH, 300 W Xe lamp with cutoff filter (λ > 440 nm),	Unclear	70	Ishii *et al.*, 2004
3	0.03 mol% La-doped, 0.2 wt.% CoO/SrTiO$_3$, with H$_2$ reduction at 773 K	Photocatalyst: 0.1 g. 800 ml of deionized water containing Na$_2$CO$_3$, 400 W high pressure Hg lamp	External irradiation	280	Qin *et al.*, 2007
4	Pt-loaded SrTiO$_3$ w/o-p-Si/Pt-loaded SrTiO$_3$	Photocatalyst: 0.05 g. 150 ml of pure water, 1 kW ultrahigh-pressure mercury arc (λ > 290 nm)	Top irradiation	12.4 28.7	Ikeda *et al.*, 2006

Table 2.2 Results of the SrTiO$_3$-based photocatalysts for photocatalytic decomposition of various pollutants

No.	Photocatalyst	Reaction	Reaction conditions	Degradation rate	References
1	Ag-doped SrTiO$_3$	Degradation of victoria blue dye	<u>Photocatalyst</u>: dye deposited film catalyst, 250 W xenon lamp and with a CuSO$_4$ solution to cut off high-UV radiation ($\lambda > 300$ nm)	The photocatalytic activity of Ag-doped SrTiO$_3$ was observed to increase the degradation of the dye by 15% when compared with native SrTiO$_3$	Subramanian et al., 2006
2	N-doped SrTiO$_3$	NO(g) elimination	<u>Photocatalyst</u>: unclear. 200 cm^3 min^{-1} of 1 ppm NO in 50 vol.% air balanced with N$_2$, 450 W high pressure Hg arc, with cutoff filter ($\lambda > 290$ nm and $\lambda > 400$ nm)	≈ 60 % conversion for $\lambda > 290$ nm and ≈ 48% conversion for $\lambda > 400$ nm	Wang et al., 2004
3	Fibrous SrTiO$_3$	NO(g) elimination	<u>Photocatalyst</u>: unclear. 200 cm^3 min^{-1} of 1 ppm NO in 50 vol.% air balanced with N$_2$, 450 W high pressure Hg arc, with cutoff filter ($\lambda > 290$ nm and $\lambda > 400$ nm)	≈ 55 % conversion for $\lambda > 290$ nm and ≈ 20 % conversion for $\lambda > 400$ nm	Wang et al., 2007
	N-doped fibrous SrTiO$_3$	NO(g) elimination		≈ 60 % conversion for $\lambda > 290$ nm and ≈ 40 % conversion for $\lambda > 400$ nm	

Table 2.2 Results of the $SrTiO_3$-based photocatalysts for photocatalytic decomposition of various pollutants (continued)

No.	Photocatalyst	Reaction	Reaction conditions	Degradation rate	References
4	$SrTiO_3$, with H_2 reduction at 773 K	Mineralization of phenol	Photocatalyst: 0.1 wt.%, 2 mM initial concentration of phenol aqueous solution with $NaClO_3$ or H_2O_2 as electron scavenger, medium pressure Hg lamp	The fraction of phenol degradation rate = 0.06, For Degussa P25, rate = 0.02	Ahuja *et al.*, 1996
5	$SrTiO_3$, 60 wt.% $CeTiO_4/SrTiO_3$, and 70 wt.% $CeTi_2O_6/SrTiO_3$	Photobleaching of methylene blue	Photocatalyst: 0.2 g, 100 ml of 2×10^{-5} mol·dm^{-3} methylene blue aqueous solution, Top irradiation of 500 W Xe lamp, with cutoff filter ($\lambda > 420$ nm)	$5.8\times10^{-3}\ \Delta_{abs}\,min^{-1}$, $6.6\times10^{-3}\ \Delta_{abs}\,min^{-1}$, $3.2\times10^{-3}\ \Delta_{abs}\,min^{-1}$, respectively	Otsuka-Yao-Matsuo *et al.*, 2004

2.6 References

Abe, R., Sayama, K., and Arakawa, H. (2003) Significant effect of iodide addition on water splitting into H_2 and O_2 over Pt-loaded TiO_2 photocatalyst: suppression of backward reaction. Chemical Physics Letters. 371, 360-364.

Abe, R., Sayama, K., and Arakawa, H. (2004) Dye-sensitized photocatalysts for efficient hydrogen production from aqueous I⁻ solution under visible light irrdition. Journal of Photochemistry and Photobiology A: Chemistry. 166, 115-122.

Ahuja, S. and Kutty, T.R.N. (1996) Nanoparticles of $SrTiO_3$ prepared by sel gel to crystallite conversion and their photocatalytic activity in the minerallization of phenol. Journal of Photochemistry and Photobiology A: Chemistry. 97, 99-107.

Anpo, M. (2004) Preparation, Characterization, and reactivities of high functional titanium oxide-based photocatalysts able to operate under UV-visible light irradiation: Approaches in Realizing high efficiency in the use of visible light. Bulletin of the Chemical Society of Japan. 77, 1427-1442.

Asahi, R., Morikawa, T., Ohwaki, T., Aoki, K., and Taga, Y. (2001) Visible light photocatalysis in nitrogen-doped titanium oxides. Science. 293, 269-271.

Ashokkumar, M. (1998) An overview on semiconductor particulate systems for photoproduction of hydrogen. International Journal of Hydrogen Energy. 23, 427-438.

Avudaithai, M. and Kutty, T.R.N. (1987) Ultrafine powders of $SrTiO_3$ prepared by hydrothermal method and their photocatalytic activity. Material Research Bulletin. 22, 641-650.

Bacsa, R.R. and Kiwi, J. (1998) Effect of rutile phase on the photocatalytic properties of nanocrystalline titania during the degradation of p-coumaric acid. Applied Catalysis B: Environmental. 16, 19-29.

Barreto, R.D., Gray, K.A., and Anders, K. (1996) Photocatalytic degradation of methyl-tert-butyl ether in TiO_2 slurries: a proposed reaction scheme. International Journal of Multiphase Flow. 22, 151-152.

Bi, Z.C. and Tien, H.T. (1984) Photoproduction of hydrogen by dye-sensitized systems. International Journal of Hydrogen Energy 9, 717-722.

Blasse, G. (1998) The influence of crystal structure on the luminescence on tantalates and niobates. Journal of Solid State Chemistry. 72, 72-79.

Bolton, J.R. (1996) Solar Photoproduction of Hydrogen: A Review. Solar Energy. 57, 37-50.

Burfeindt, B., Hannappel, T., Storck, W., and Willig, F. (1996) Measurement of temperature-independent femtosecond interfacial electron transfer from an anchored molecular electron donor to a semiconductor as acceptor. Journal of Physical Chemistry. 100, 16461-16465.

Cales, B.J. and Baumard, F. (1984) Mixed conduction and defect structure of ZrO_2-CeO_2-Y_2O_3 solid solution. Journal of the Electrochemical Society. 131, 2407-2413.

Chavadej, S., Phuaphromyod, P., Gulari, E., Rangsunvigit, P., and Sreethawong, T. (2008) Photocatalytic degradation of 2-propanol by using Pt/TiO_2 prepared by microemulsion technique. Chemical Engineering Journal. 137, 489-495.

Dai, Q., Zhang, Z., He, N., Li, P., and Yuan, C. (1999) Preparation and characterization of mesostructured titanium dioxide and its application as a photocatalyst for the wastewater treatment. Materials Science and Engineering C. 8-9, 417-423.

De, G.C., Roy, A.M., and Bhattacharya, S.S. (1996) Effect of n-Si on the photocatalytic production of hydrogen by Pt-loaded CdS and CdS-ZnS catalysts. International Journal of Hydrogen Energy. 21, 19-23.

Domen, K., Kudo, A., and Onishi, T. (1986) Mechanism of photocatalytic decomposition of water into H_2 and O_2 over NiO-$SrTiO_3$. Journal of Catalysis. 102, 92-98.

Gurunathan, K., Maruthamuthu, P., and Sastri, V.C. (1997) Photocatalytic hydrogen production by dye-sensitized Pt/SnO_2 and $Pt/SnO_2/RuO_2$ in aqueous methyl viologen solution. International Journal of Hydrogen Energy 22, 57-62.

Hannappel, T., Burfeindt, B., and Storck, W. (1997) Measurement of ultrafast photoinduced electron transfer from chemically anchored Ru-dye molecules

into empty electronic states in a colloidal anatase TiO_2 film. Journal of Physical Chemistry B. 101, 6799-6802.

Hoffmann, M.R., Balcerski, W., and Ryu, S. (2008) Gas-phase photodegradation of decane and methanol on TiO_2: dynamic surface chemistry characterized by diffuse reflectance FTIR-SP2. International Journal of Photoenergy. Accepted 4 Jan. 2008 (doi:10.1155/2008/964721).

Honda, K. and Fujishima, A. (1972) Electrochemical photolysis of water at a semiconductor electrode. Nature. 238, 37-38.

Hotchandani, S. and Kamat, P.V. (1992) Charge-transfer processes in coupled semiconductor systems: photochemistry and photoelectrochemistry of the colloidal CdS-ZnO system. Journal of Physical Chemistry. 96, 6834-6839.

Ikeda, S., Hirao, K., Ishino, S., Matsumura, M., and Ohtani, B. (2006) Preparation of platinized strontium titanate covered with hollow silica and its activity for overall water splitting in a novel phase-boundary photocatalytic system. Catalysis Today. 117, 343–349.

Ishii, T., Kato, H., and Kudo, A. (2004) H_2 evolution from an aqueous methanol solution on $SrTiO_3$ photocatalysts codoped with chromium and tantalum ions under visible light irradiation. Journal of Photochemistry and Photobiology A: Chemistry. 163, 181-186.

Jang, J.S., Ji, S.M., Bae, S.W., Son, H.C., and Lee, J.S. (2007) Optimization of CdS/TiO_2 nano-bulk composite photocatalysts for hydrogen production from Na_2S/Na_2SO_3 aqueous electrolyte solution under visible light ($\lambda \geq 420$ nm). Journal of Photochemistry and Photobiology A: Chemistry. 188, 112-119.

Jin, Z., Zhang, X., Li, Y., Li, S., and Lu, G. (2007) 5.1% Apparent quantum efficiency for stable hydrogen generation over eosin-sensitized CuO/TiO_2 photocatalyst under visible light irradiation. Catalysis Communications. 8, 1267-1273.

Kajiwara, T., Hashimoto, K., Kawai, T., and Sakata, T. (1982) Dynamics of luminescence from $Ru(bpy)_3Cl_2$ adsorbed on semiconductor surfaces. Journal of Physical Chemistry. 86, 4516-4522.

Kamat, P.V. (1999) Handbook of Nanostructured Materials and Nanotechnology: Semiconductor Nanoparticles, Academic Press, New York, 292-234.

Kiwi, J. and Gratzel, M. (1979) Projection, size factors, and reaction dynamics of colloidal redox catalysts mediating light induced hydrogen evolution from water. Journal of the American Chemical Society. 101, 7214-7217.

Konta, R., Ishii, T., Kato, H., and Kudo, A. (2004) Photocatalytic activities of noble metal ion doped $SrTiO_3$ under visible light irradiation. Journal of Physical Chemistry B. 108, 8992-8995.

Kudo, A., Kato, H., and Nakagawa, S. (2000) Water splitting into H_2 and O_2 on new $Sr_2M_2O_7$ (M = Nb and Ta) photocatalysts with layered perovskite structures: factors affecting the photocatalytic activity. Journal of Physical Chemistry B. 104, 571-575.

Kudo, A., Kato, H., and Tuji, I. (2004) Strategies for the development of visible-light-driven photocatalysts for water splitting. Chemistry Letters. 33, 1534-1541.

Kudo, A. (2006) Development of photocatalyst materials form water splitting. International Journal of Hydrogen Energy. 31, 197-202.

Kutty, T. R. N. and Avudaithai, M. (1988) Sacrificial photolysis of water on TiO_2 fine powders prepared by the hydrothermal method. Materials Research Bulletin. 23, 725-734.

Li, Y.X., Lu, G.X., and Li, S.B. (2003) Photocatalytic production of hydrogen in single component and mixture systems of electron donors and monitoring adsorption of donors by in situ infrared spectroscopy. Chemosphere. 52, 843-850.

Licht, S., Wang, B., Mukerji, S., Soga, I.T., Umeno, M., and Tributsch, H. (2000) Efficient solar water splitting, exemplified by RuO_2-catalyzed AlGaAs/Si photoelectrolysis. Journal of Physical Chemistry B. 104, 8920-8924.

Linsebigler, A.L., Lu, G., Yates, J.T. (1995) Photocatalysis on TiO_2 surfaces: principles, mechanisms, and selected results. Chemical Reviews. 95, 735-758.

Martini, I., Hodak, J.H., and Hartland, G.V. (1998) Effect of water on the electron transfer dynamics of 9-anthracenecarboxylic acid bound to TiO_2

nanoparticles: demonstration of the Marcus inverted region. Journal of Physical Chemistry B. 102, 607-614.

Meissner, D. (1999) Solar technology: photoelectrochemical solar energy conversion. Ullmann Encyclopedia of Industrial Chemistry. 6.

Memming, R. (1983) Progress in Surface Science, Pergamon, Oxford. 17, 7-74.

Naito, H. and Arashi, H. (1995) Hydrogen production from direct water splitting at high temperatures using a ZrO_2-TiO_2-Y_2O_3 membrane. Solid State Ionics. 79, 366-370.

Ohno, T., Akiyoshi, M., Umebayashi, T., Asai, K., Mitsui, T., and Matsumura, M. (2004) Preparation of S-doped TiO_2 photocatalysts and their photocatalytic activities under visible light. Applied Catalysis A: General. 265, 115-121.

Otsuka-Yao-Matsuo, S., Omata, T., and Yoshimura, M. (2004) Photocatalytic behavior of cerium titanates, $CeTiO_4$ and $CeTi_2O_6$ and their composite powders with $SrTiO_3$. Journal of Alloys and Compounds. 376, 262–267.

Patsoura, A., Kondarides, D.I., and Verykios, X.E. (2007) Photocatalytic degradation of organic pollutants with simultaneous production of hydrogen. Catalysis Today. 124, 94-102.

Pozdnyakov, I.P., Sosedova, Yu.A., Plyusnin, V.F., Glebov, E.M., Grivin, V.P., Vorobyev, D.Yu., and Bazhin, N.M. (2004) Photodegradation of organic pollutants in aqueous solutions caused by $Fe(OH)^{2+}$ aqueous solution photolysis: evidence of OH radical formation. International Journal of Photoenergy. 6, 89-93.

Qin, Y., Wang, G., and Wang, Y. (2007) Study on the photocatalytic property of La-doped CoO/$SrTiO_3$ for water decomposition to hydrogen. Catalysis Communications. 8, 926-930.

Rehm, J.M., Mclendon, G.L., Nagasawa, Y., Yoshihara, K., Moser, J., and Gratzel, M. (1996) Femtosecond electron-transfer dynamics at a sensitizing dye-semiconductor (TiO_2) interface. Journal of Physical Chemistry. 100, 9577-9578.

Rouquerol, F., Rouquerol, J., and Sing, K. (1999) Adsorption by Powders and Porous Solids: Principles, Methodology and Applications, Academic Press, San Diego.

Sayama, K. and Arakawa, H. (1992) Significant effect of carbonate addition on stoichiometric photodecomposition of liquid water into hydrogen and oxygen from platinum-titanium (IV) oxide suspension. Journal of Chemical Society: Chemical Communications. 2, 150-152.

Sayama, K. and Arakawa, H. (1994) Effect of Na_2CO_3 addition on photocatalytic decomposition of liquid water over various semiconductors catalysis. Journal of Photochemistry and Photobiology A: Chemistry. 77, 243-247.

Sayama, K. and Arakawa, H. (1996) Effect of carbonate addition on the photocatalytic decomposition of liquid water over a ZrO_2 catalyst. Journal of Photochemistry and Photobiology A: Chemistry. 94, 67-76.

Sayama, K. and Arakawa, H. (2000) Solar hydrogen production: significant effect of Na_2CO_3 addition on water splitting using simple oxide semiconductor photocatalysts. Catalysis Surveys from Japan. 4, 75-80.

Sayama, K., Mukasa, K., Abe, R., Abe, Y., and Arakawa, H. (2002) A new photocatalytic water splitting system under visible light irradiation mimicking a Z-scheme mechanism in photosynthesis. Journal of Photochemistry and Photobiology A: Chemistry. 148, 71-77.

So, W.W., Kim, K.J., and Moon, S.J. (2004) Photo-production of hydrogen over the CdS-TiO_2 nano-composite particulate films treated with $TiCl_4$. International Journal of Hydrogen Energy. 29, 229-234.

Sreethawong, T., Suzuki, Y., and Yoshikawa, S. (2005) Photocatalytic evolution of hydrogen over mesoporous TiO_2 supported NiO photocatalyst prepared by single-step sol–gel process with surfactant template, International Journal of Hydrogen Energy. 30, 1053-1062. a

Sreethawong, T., Ngamsinlapasathian, S., Suzuki, Y., and Yoshikawa, S. (2005) Nanocrystalline mesoporous Ta_2O_5-based photocatalysts prepared by surfactant-assisted templating sol-gel process for photocatalytic H_2 evolution. Journal of Molecular Catalysis A: Chemical. 235, 1-11. b

Sreethawong, T., Yamada, Y., Kobayashi, T., and Yoshikawa, S. (2005) Catalysis of nanocrystalline mesoporous TiO_2 on cyclohexene epoxidation with H_2O_2: Effects of mesoporosity and metal oxide additives. Journal of Molecular Catalysis A: Chemical. 241, 23-32. c

Sreethawong, T. and Yoshikawa, S. (2006), Enhanced photocatalytic hydrogen evolution over Pt supported on mesoporous TiO_2 prepared by single-step sol–gel process with surfactant template. International Journal of Hydrogen Energy. 31, 786-796.

Subramanian, V., Roeder, R.K., and Wolf, E.E. (2006) Synthesis and UV-visible-light photoactivity of noble-metal-$SrTiO_3$ composites. Industrial Engineering Chemical Research. 45, 2187-2193.

Suzuki, T., Jasinski, P., Petrovsky, V., and Anderson, H.U. (2005) The optical properties and band gap energy of nanocrystalline $La_{0.4}Sr_{0.6}TiO_3$ thin films. Journal of the American Ceramic Society. 88, 1186–1189.

Takata, T., Tanaka, A., Hara, M., Kondo, J.N., and Domen, K. (1998) Recent progess of photocatalysts for overall water splitting. Catalysis Today. 44, 17-26.

Torres, G.R., Lindgren, T., Lu, J., Granqvist, C.G., and Lindquist, S.E. (2004) Photoelectrochemical study of nitrogen-doped titanium dioxide for water oxidation. Journal of Physical Chemistry B. 108, 5995-6003.

Tsuji, I. and Kudo, A. (2003) Hydrogen evolution from aqueous sulfite solutions under visible light irradiation over Pb and halogen-codoped ZnS photocatalysts. Journal of Photochemistry and Photobiology A: Chemistry. 156, 249-252.

Wang, J., Yin, S., Komatsu, M., Zhang, Q.W., Saito, F., and Sato, T. (2004) Preparation and characterization of nitrogen doped $SrTiO_3$ photocatalyst. Journal of photochemistry and Photobiology A: Chemistry. 165, 149-156.

Wang, J., Yin, S., Komatus, M., and Sato, T. (2005) Lanthanum and nitrogen co-doped $SrTiO_3$ powders as visible light sensitive photocatalyst. Journal of European Ceramic Society. 25, 3207-3212.

Wang, J., Yin, S., and Sato T. (2007) Characterization and evaluation of fibrous $SrTiO_3$ prepared by hydrothermal process for the destruction of NO. Journal of Photochemistry and Photobiology A: Chemistry. 187, 72-77.

Wang, P., Zakeeruddin, S.M., and Gratzel, M. (2003) Solar cell: A solid compromise: Article. Nature Material. 2, 402-407.

Yan, S.G. and Hupp, J.T. (1996) Semiconductor-based interfacial electron-transfer reactivity: decoupling kinetics from pH-dependent band energetic in a dye-sensitized titanium dioxide/aqueous solution system. Journal of Physical Chemistry. 100, 6867-6870.

Zou, Z., Ye, J., and Arakawa, H. (2003) Photocatalytic water splitting into H_2 and/or O_2 under UV and visible light irradiation with semiconductor photocatalyst. International Journal of Hydrogen Energy. 28, 663-669.